ISSN 1063-7761, Journal of Experimental and Theoretical Physics, 2021, Vol. 133, No. 6, pp. 771–778. © Pleiades Publishing, Inc., 2021.
Russian Text © The Author(s), 2021, published in Zhurnal Eksperimental'noi i Teoreticheskoi Fiziki, 2021, Vol. 160, No. 6, pp. 903–911.

ORDER, DISORDER, AND PHASE TRANSITION IN CONDENSED SYSTEM

High-Field Magnetoresistance of Magnetic Nanocomposites near the Percolation Threshold

E. A. Fadeev[a,*], M. A. Shakhov[b], E. Lähderanta[a,], A. N. Taldenkov[c], A. L. Vasiliev[c,d], A. V. Sitnikov[e], V. V. Rylkov[c,f], and A. B. Granovsky[f,g]**

[a] *Lappeenranta-Lahti University of Technology LUT, Lappeenranta, 53850 Finland*
[b] *Ioffe Institute, St. Petersburg, 194021 Russia*
[c] *National Research Center "Kurchatov Institute," Moscow, 123098 Russia*
[d] *Moscow Institute of Physics and Technology (MIPT), Dolgoprudny, Moscow oblast, 141701 Russia*
[e] *Voronezh State Technical University, Voronezh, 394026 Russia*
[f] *Institute of Applied and Theoretical Electrodynamics RAS, Moscow, 127412 Russia*
[g] *Faculty of Physics, Moscow State University, Moscow, 119991 Russia*
** e-mail: egor.fadeev@lut.fi*
*** e-mail: erkki.lahderanta@lut.fi*

Received July 15, 2021; revised July 15, 2021; accepted August 23, 2021

Abstract—We present results of experimental studies of high-field magnetoresistance of Co–SiO_2, Co–$LiNbO_3$, CoNbTa–SiO_2 nanocomposites with metal volume fraction close to the percolation threshold. The nanocomposite films were deposited onto a glass-ceramic substrate by ion-beam sputtering at the growth temperature not exceeding 80°C. Magnetization was measured using a superconducting quantum interference device (SQUID) magnetometer in the temperature range of 4.2–300 K. Out-of-plane magnetoresistance was measured in a pulsed magnetic field up to 20 T in the temperature range of 4.2–300 K with the pulse duration of 11–12 ms. In addition to negative magnetoresistance, a linear positive contribution to magnetoresistance was observed in high magnetic fields for nanocomposites with the composition close to the percolation threshold. This effect was explained by the influence of the Zeeman effect on the tunnel barrier height. It is shown that the unconventional anisotropy of magnetoresistance of Co–$LiNbO_3$ is associated with the peculiarities of its microstructure.

DOI: 10.1134/S1063776121120049

1. INTRODUCTION

The discovery of linear positive magnetoresistance (LPMR) in high magnetic fields in a variety of ferromagnetic materials, composites and manganites ([1, 2] and references therein) has induced significant interest. This is mainly because LPMR could not be explained by known mechanisms of magnetoresistance (MR) in magnetic materials [1, 2], in which MR is commonly negative and anisotropic in the magnetic fields lower than a saturation field. LPMR is isotropic and it does not show signatures of saturation even in magnetic fields up to 60 T. Potentially it can be used as a basis for the development of high magnetic field sensors. LPMR was not observed in chemically homogeneous bulk magnetic materials nor in paramagnetic thin films [1]; only inhomogeneous magnetic materials such as deposited polycrystalline thin films of ferromagnetic materials (Ni, Fe, Co) or magnetic nanocomposites demonstrate the effect [1, 2]. Commonly, LPMR value does not exceed 0.001–0.01% T^{-1}, however, in weakly conductive Ni films mixed with insulating SiO_2 LPMR reaches a value of 0.1% T^{-1} [1].

It is still unclear, whether LPMR is a result of only one mechanism or not. In [1], the LPMR is explained by the influence of the Zeeman effect on the quantum corrections to resistivity, which are caused by electron–electron interaction. However, as the authors themselves mentioned, the proposed mechanism can not explain the magnitude of the effect. Moreover, LPMR takes place in systems without any indication of the contribution of the quantum corrections to resistivity. In [2], the LPMR is associated with the influence of the Zeeman effect on the tunnel barrier height in the case of spin-polarized tunneling. This mechanism is universal since tunneling takes place in a variety of materials such as island and polycrystalline films, nanocomposites with concentrations close to the percolation threshold, binary structures, etc. To explain the LPMR behavior, authors of [2] derived a simple expression based on the Inoue–Maekawa model of tunneling MR in granular films [3]. This

expression allowed them to explain qualitatively the LPMR results of $(Co_{40}Fe_{40}B_{20})_x(SiO_2)_{100-x}$ and $(Co_{84}Nb_{14}Ta_2)_x(Al_2O_3)_{100-x}$ nanocomposites [2]. However, the Inoue-Maekawa model is valid only for nanocomposites with a composition below a metal-insulator transition (MIT), whose temperature dependence of resistivity follows "$T^{1/2}$" law ($\ln\rho \propto T^{-1/2}$), whereas the temperature dependence of resistivity of the studied nanocomposites follows "$\ln T$" law ($\rho \propto \ln T$) [2]. Commonly, such behavior is observed for metal concentrations above the MIT (x_c), but below the percolation threshold (x_p), and corresponds to conductivity of "dirty metal" with strong tunnel coupling between granules. Moreover, in [2], the MR curves of the studied samples were measured only at $T > 65$ K.

In the present paper, we continue search for and investigation of LPMR in nanocomposite materials. New compounds were fabricated with material variation of both magnetic granules and dielectric matrices. MR was measured in pulsed magnetic fields at the temperatures down to 4.2 K. The expression from [2] was modified for "metallic" side from the MIT with the "$\ln T$" law.

2. EXPERIMENTAL

Nanocomposite Co–SiO_2, Co–$LiNbO_3$, CoNbTa–SiO_2 films with a thickness of 1.7 μm were fabricated by ion-beam sputtering of components' targets onto a glass-ceramic substrate at the temperature not exceeding 80°C. Details of fabrication, elemental composition investigation, and structural characterization are the same as in [3, 4]. Concentration of the metallic granules varied from the "metallic" region to the concentrations corresponding to the MIT. Magnetization was measured using a SQUID magnetometer (Quantum Design MPMS-XL7). The temperature dependences of resistivity in the range of 50–300 K were recorded with a standard DC four-probe method. Pulsed magnetic fields up to 20 T were applied to measure MR. A symmetric ("half-sine shaped") pulse was used with a duration of 11–12 ms. Special hardware and software were used to exclude parasitic signals induced by dB/dt (see details in [5]).

To study structural properties of the fabricated samples, cross-sectional lamellae of the nanocomposite films were prepared using a focused ion beam (FIB) Ga^+ system in a scanning electron microscope (SEM)/FIB "Helios NanoLab™ 600i" (Thermo Fisher Scientific, USA). High-resolution images were obtained using a scanning/transmission electron microscope (S/TEM) "Tecnai Osiris" (Thermo Fisher Scientific, USA) operating at 200 kV equipped with energy dispersive X-ray spectrometer (EDXS) "Super-X" (Bruker, USA) and high-angle annular dark-field detector (HAADF) (Fischione, USA).

3. RESULTS AND DISCUSSION

The magnetic hysteresis loops of the studied samples are typical for magnetic nanocomposites and are presented in Fig. 1. The hysteresis loops converge in $H \approx 2$–3 kOe, but at low temperatures and in high magnetic fields, magnetization continues to grow due to the presence of superparamagnetic granules and magnetic ions, dispersed in the dielectric matrix [3, 6]. In magnetic fields lower than the saturation ones ($H_{sat} \approx 2$–4 kOe), the MR is negative and its magnitude rises sharply with magnetic field (Figs. 2–4). Nonetheless, in $H > H_{sat}$, the negative MR continues to grow, which is typical for tunneling MR with the presence of superparamagnetic granules (Figs. 2–4). The LPMR is observed only at low temperatures (Figs. 2–4).

At $T = 4.2$ K, the LPMR of Co–SiO_2 and CoNbTa–SiO_2 is 0.03 and 0.06% T^{-1}, respectively. The order of magnitude agrees with the results of the papers [1, 2]. In the Co–$LiNbO_3$ film, at $T = 50$ K, the LPMR is less by the order of magnitude. We were not able to measure MR of the Co–$LiNbO_3$ nanocomposite at $T < 50$ K due to the sharp rise of resistance at the lower temperatures. To discuss and analyze the obtained data we modify the theory developed in [2] and we take into account the differences in structure, magnetic properties, and conductivity of the studied magnetic nanocomposites.

As mentioned above, there are two possible conductivity regimes for nanogranular films with concentrations near the MIT ($x \approx x_c$). The first regime ($x \le x_c$) takes place when average tunneling conductance between adjacent granules (G_t) is less than the conductance quantum ($G_q = 2e^2/h$), meaning $g = G_t/G_q < 1$, then conductivity σ is described by the "$T^{1/2}$" law,

$$\ln\sigma \propto \left(\frac{T_0}{T}\right)^{1/2}. \quad (1)$$

The second regime ($x_c \le x \le x_p$) is observed when $g = G_t/G_q \gg 1$ with strong tunnel coupling between granules at the slightly elevated metal concentration in comparison to the first regime. The second regime is described by the "$\ln T$" law [5, 7],

$$\sigma(T) = \sigma_0\left(1 - \frac{1}{2\pi Dg}\ln\frac{gE_c}{k_BT}\right), \quad (2)$$

where σ_0 is nanocomposite conductivity at relatively high temperature when it is possible to neglect the effect of Coulomb interaction, and D is dimensionality of the system. The Coulomb blockade energy can be written as

$$E_c = \frac{e^2 s}{\epsilon_d a^2(1/2 + s/a)}, \quad (3)$$

where a is diameter of a granule, s is tunnel gap width and ϵ_d is permittivity of the matrix [8].

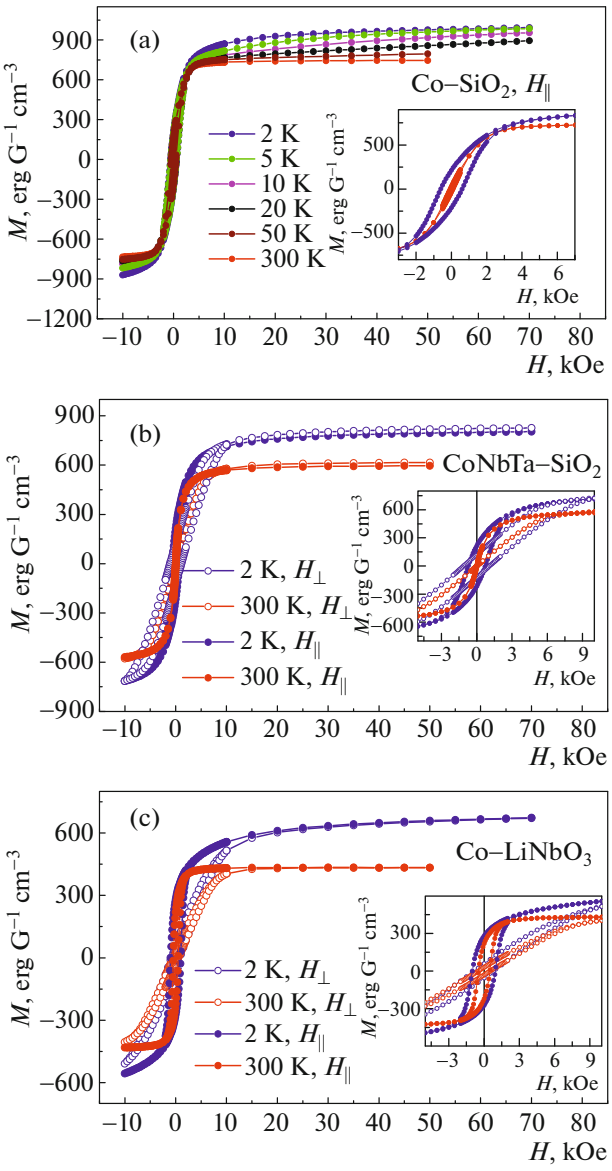

Fig. 1. Magnetic hysteresis loops of the studied nanocomposites at different temperatures and orientations. The inserts show different scales of the same curves.

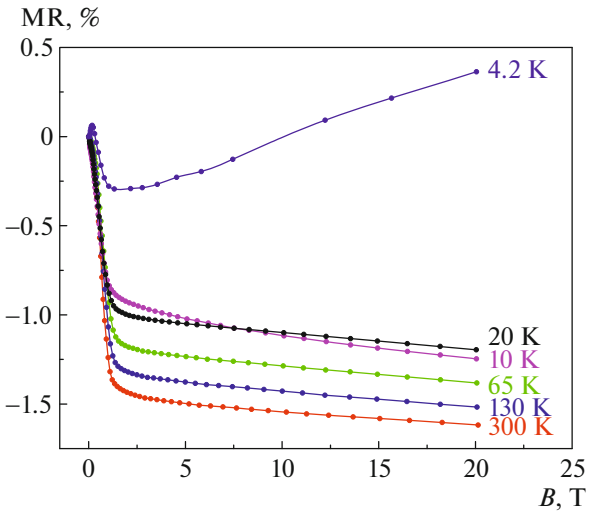

Fig. 2. Out-of-plane MR of $(Co)_x(SiO_2)_{100-x}$ with x = 65 at %.

For the first regime, in the framework of the Inoue–Maekawa model, authors of [2] have derived the expression for LPMR based on the influence of the Zeeman effect on the tunnel barrier height. At low temperatures, this expression takes form

$$\frac{\Delta\rho(H)}{\rho(0)} = \frac{\rho(H)-\rho(H=0)}{\rho(H=0)} = \xi\frac{\mu_B H}{U-E_F(0)}\sqrt{\frac{\lambda C}{k_B T}}, \quad (4)$$

where $C = sE_c$, k_B is the Boltzmann constant, and the Fermi energy depends on the applied magnetic field as

$$E_F(H) = E_F(0) - \xi\mu_B H. \quad (5)$$

Here ξ is a parameter that characterizes a shift of the Fermi level and is equal in the magnitude to spin polarization P, and μ_B is the Bohr magneton. The parameter

$$\lambda = \sqrt{\frac{2m}{\hbar^2}(U-E_F(0))},$$
$$\lambda(H) = \sqrt{\frac{2m}{\hbar}(U-E_F(0)+\xi\mu_B H)} \quad (6)$$

characterizes a wave function decay of a tunneling electron in a barrier with the height of $U - E_F(0)$.

For the second regime, conductance can be written as follows

$$g(H) \propto (1+P^2m^2)e^{-2\lambda(H)s}, \quad (7)$$

where m is relative magnetization, which in saturation equals to 1 [9]. Then, the Fermi level shifts under the influence of the Zeeman effect (5), and using (2), (5)–(7) we derive the expression for LPMR in $H > H_{sat}$:

$$\frac{\Delta\rho(H)}{\rho(H)} = \xi\frac{\mu_B H}{U-E_F(0)}\frac{\lambda s}{2\pi Dg}\left[\ln\left(\frac{gE_c}{k_B T}\right)-1\right]. \quad (8)$$

Both (4) and (8) give the same order of magnitude but different temperature dependences of LPMR. For $a \approx$ 3 nm, $s \approx 1$ nm, $D = 3$ and $d \approx 3.75$ (for SiO_2) one has $E_c \approx 51.5$ meV, and then for $U - E_F = 1.0$ eV and $g =$ 1.0, at $T = 4.2$ K, the LPMR $\frac{\Delta\rho(H)}{\rho(0)} \approx 0.01\%$ T^{-1}. We emphasize that in the second regime it is the maximum value of LPMR at $U - E_F = 1.0$ eV and $g = 1.0$, since we assumed that $\xi = 1$, which implies 100% spin polarization. At $U - E_F = 0.1$ eV and with the rest parameters being the same, the LPMR is increased by

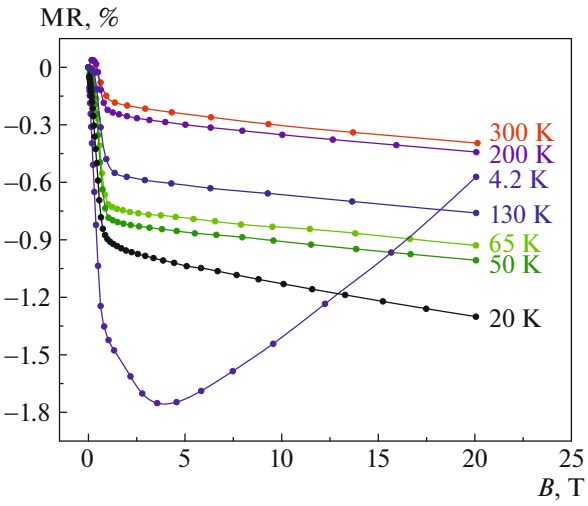

Fig. 3. Out-of-plane MR of $(CoNbTa)_x(SiO_2)_{100-x}$ with $x = 58.5$ at %.

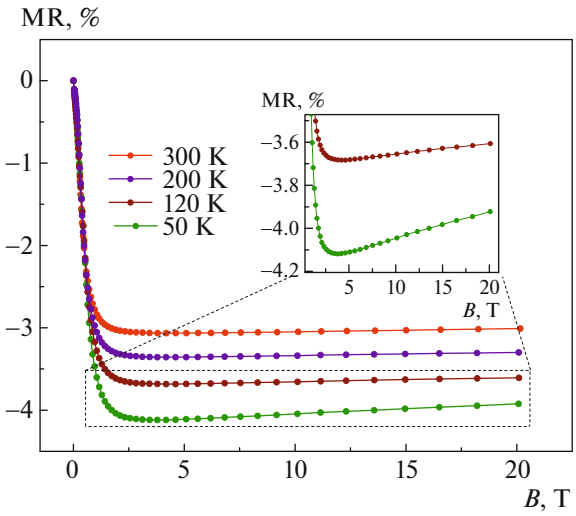

Fig. 4. Out-of-plane MR of $(Co)_x(LiNbO_3)_{100-x}$ with $x =$ 49 at %.

3.3 times, whereas at $U - E_F = 0.1$ eV and $g = 10$, $\frac{\Delta\rho(H)}{\rho(0)} \approx 0.1\%\ T^{-1}$.

Presented in [2] the LPMR results at $T = 65$ K of the nanocomposites CoFeB–SiO_2 and CoNbTa–Al_2O_3 are characterized by the "ln$T$" law and lie within the range of $\frac{\Delta\rho(H)}{\rho(0)} \approx 10^{-3}$–$10^{-4}\%\ T^{-1}$. These values correspond to the calculation results using the obtained expression (8). Note that signatures of quantum corrections for the nanocomposites in [2] were not observed, which excludes the mechanism of LPMR proposed in [1].

3.1. $(Co)_x(SiO_2)_{100-x}$

The LPMR is observed only for the composition with $x = 65$ at % and its magnitude is $0.03\%\ T^{-1}$ (Fig. 2). Temperature dependences of resistivity of the studied nanocomposites are presented in Figs. 5–7. For the $(Co)_x(SiO_2)_{100-x}$ with $x = 65$ at %, the "ln$T$" law describes the data better than the "$T^{1/2}$" law (Fig. 5). As can be seen from the slope of the curves $1/2\pi Dg$ in Fig. 5, for this composition, $g \approx 1$ at $D = 3$. However, as noted in [3], for the considered model $2D$ is equal to the number of the nearest granules (Z) between which tunneling is possible, that is, for the disordered case $D < 3$. Therefore, for the composition with $x = 65$ at %, $g > 1$, and we can use the expression (8), which correctly describes the obtained data.

As can be seen from Fig. 2, the negative MR is higher at $T = 300$ K than at low temperatures. To explain this anomaly we should take into account possibility of formation of granules and aggregates at the concentrations close to the MIT. This may induce not only tunneling MR, but also negative MR due to suppression of magnetic disorder in the granules. The latter contribution can be of the same magnitude as negative tunneling MR and it rises with temperature due to an increase of spin fluctuations. The data from electron microscopy of the studied nanocomposites confirms the presence of such aggregates. Moreover, the metal concentration in the vicinity of the percolation threshold of the nanocomposite in Fig. 2 is higher than the concentration of the other studied nanocomposites. This indirectly confirms the presence of the aggregates. In addition, in $H > H_{sat}$ and at low temperatures, positive contribution to MR, due to the effect of magnetic blockade, is possible [9], which diminishes the negative MR at low temperatures.

3.2. $(CoNbTa)_x(SiO_2)_{100-x}$

For the nanocomposite $(CoNbTa)_x(SiO_2)_{100-x}$ with $x = 58.5$ at %, metal concentration is lower than in the previous sample, and resistivity is well described by the "ln$T$" law (Fig. 6). Concentration change of ions dispersed in dielectric matrix and composition variation of ferromagnetic granules can change the tunnel barrier height and spin polarization, leading to the increase of the LPMR up to $\frac{\Delta\rho(H)}{\rho(0)} \approx 0.06\%\ T^{-1}$. This magnitude is the highest among all the nanocomposites studied.

It should be noted that LPMR, according to the proposed mechanism, is extremely sensitive to the concentration of dispersed magnetic and nonmagnetic ions in the tunnel gap. On the one hand, such ions can decrease the tunnel barrier height, but on the other hand, by changing the permittivity of the matrix, their presence can reduce the Coulomb blockade

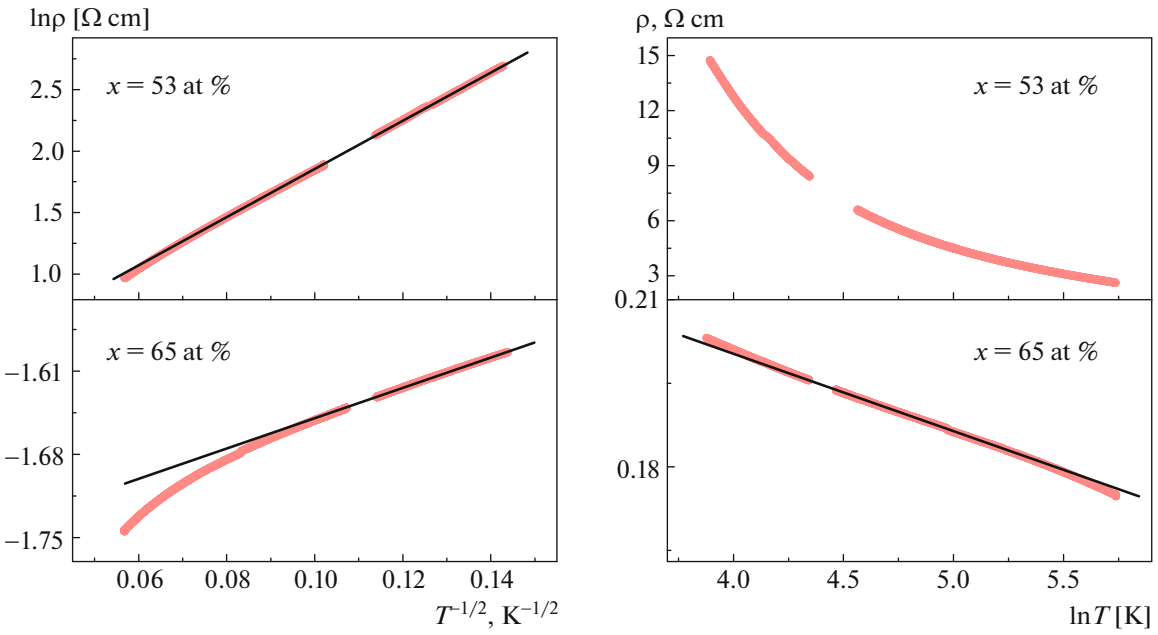

Fig. 5. Temperature dependences of resistivity of the $(Co)_x(SiO_2)_{100-x}$ nanocomposite. The left column represents $\ln\rho \propto T^{-1/2}$ behavior, the right column represents $\rho \propto \ln T$ behavior. The black solid lines are linear fits.

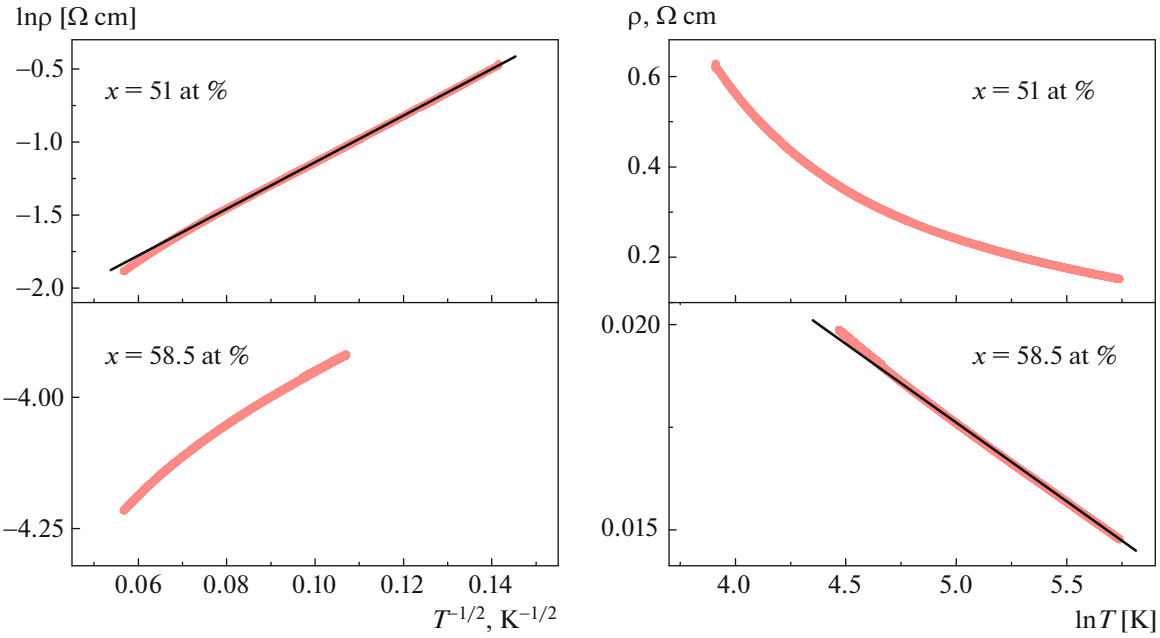

Fig. 6. Temperature dependences of resistivity of the $(CoNbTa)_x(SiO_2)_{100-x}$ nanocomposite. The left column represents $\ln\rho \propto T^{-1/2}$ behavior, the right column represents $\rho \propto \ln T$ behavior. The black solid lines are linear fits.

energy and also lead to the absence of magnetic and MR saturation in high magnetic fields. Presumably, that is the reason why the LPMR of the $(Co)_x(SiO_2)_{100-x}$ and $(CoNbTa)_x(SiO_2)_{100-x}$ nanocomposites takes place at $T = 4.2$ K, but is not observed already at $T = 10$ K even though (3) and (8) do not predict strong temperature dependence. Indeed, the studied nanocomposites are fabricated at the elevated temperature of the substrate (80°C), which makes their microstructure, and hence magnetic properties, to be different from the ones studied in [2]. For example, the magnetization of the $(Co)_x(SiO_2)_{100-x}$ nanocomposite saturates at $T = 2$ K

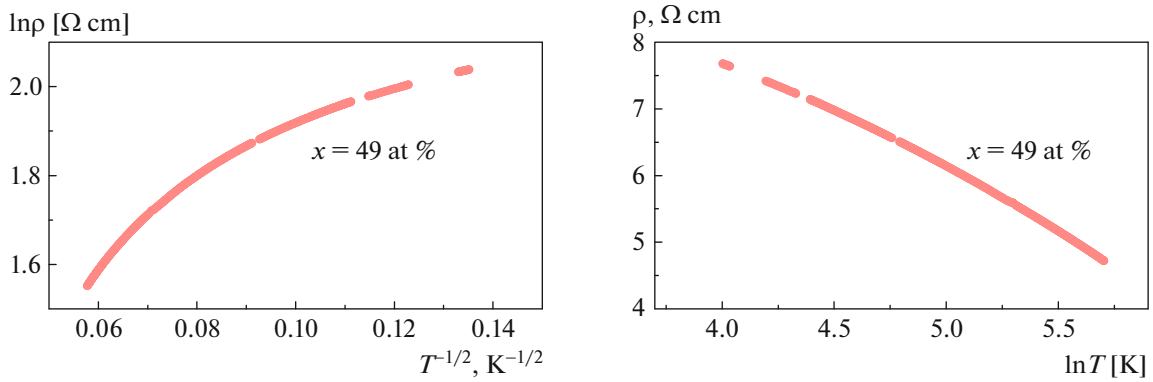

Fig. 7. Temperature dependences of resistivity of the $(Co)_x(LiNbO_3)_{100-x}$ nanocomposite. The left column represents $\ln\rho \propto T^{-1/2}$ behavior, the right column represents $\rho \propto \ln T$ behavior.

in $H \approx 4$ kOe, but at higher magnetic fields, the magnetization continues to grow (Fig. 1), which means a rise of the negative tunneling contribution to the MR. With the increased negative tunneling contribution, the positive contribution to the MR becomes indistinguishable. Therefore, the major reason why LPMR is not visible at $T > 4.2$ K is the strong competitive negative contribution to MR in high magnetic fields due to the presence of superparamagnetic granules and dispersed ions.

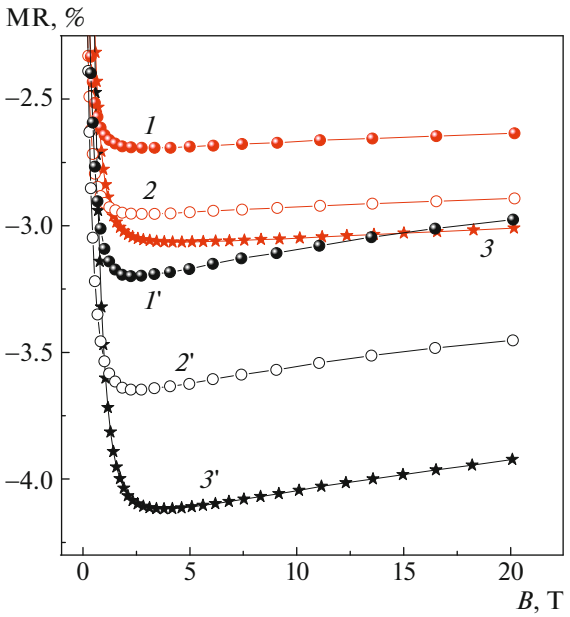

Fig. 8. Magnetoresistance of the $(Co)_x(LiNbO_3)_{100-x}$ nanocomposite with $x = 49$ at % at different orientations of the magnetic field to the sample plane and current direction: *1*, *1'*—magnetic field is parallel to both sample plane and current direction; *2*, *2'*—magnetic field is parallel to sample plane and perpendicular to current direction; *3*, *3'*—magnetic field is perpendicular to both sample plane and current direction. Curves with and without prime are measured at $T = 50$ and 300 K, respectively.

3.3. $(Co)_x(LiNbO_3)_{100-x}$

The conductivity of the nanocomposite Co–$LiNbO_3$ does not follow either "$\ln T$" or "$T^{1/2}$" laws (Fig. 7), nevertheless, in Fig. 4 one can see the signatures of positive MR in high magnetic fields for the composition with $x = 49$ at %. The LPMR is of the order of 10^{-3}% T^{-1}, which is similar value to the composites CoFeB–SiO_2 and CoNbTa–Al_2O_3, however, the MR of Co–$LiNbO_3$, in contrast to other studied samples, is anisotropic. The in-plane MR (magnetic field oriented parallel to the sample plane) is higher when magnetic field is oriented perpendicular to the current direction rather than parallel. Additionally, when magnetic field is perpendicular to the current direction, the in-plane MR differs from the out-of-plane MR (Fig. 8). Neither of these features were observed in the previous two samples nor in the samples of [1]. It would be natural to connect these features with microstructure properties of the Co–$LiNbO_3$ nanocomposite, which is discussed below.

The results of STEM/TEM study of the Co–$LiNbO_3$ nanocomposite are presented in Fig. 9, where one can see a columnar structure near the interface between $(Co)_x(LiNbO_3)_{100-x}$ and the glass-ceramic substrate. The structure consists of cobalt granules, elongated mainly in the direction of nanocomposite growth with a lateral size in the film plane of 5–8 nm (Fig. 9, image B). Vertical growth continues up to ~20 nm, where the columnar granules start to bend (Fig. 9). Above the columnar structure layer (~100 nm thick), an amorphous-crystalline nanocomposite is formed, consisting of spherical crystalline nanoparticles with a size of 5–30 nm, separated by an amorphous interlayer. The high-resolution TEM results together with EDXS mapping (not shown here) demonstrated that the crystalline particles and the interlayer consist of

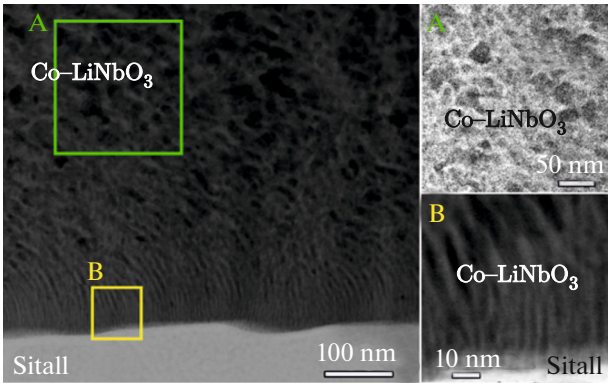

Fig. 9. Bright-field STEM image of a cross-section of $(Co)_x(LiNbO_3)_{100-x}$ film (x = 49 at %) on the glass-ceramic substrate (left side). Top right image (A) shows a dark-field TEM image obtained using hollow cone illumination mode with the objective aperture set in the diffuse background area. Such mode leads to bright contrast of amorphous layer in between the crystalline Co particles. Bottom right image (B) shows a bright-field STEM image of the interface area. The elongated grains up to 20–25 nm forming from the interface are clearly visible.

Co and amorphous $LiNbO_3$, respectively. The high defectiveness of Co nanoparticles should be noted, consisting of stacking faults and twins, which is typical for Co nanoparticles. A similar columnar structure was observed earlier in the $(CoFeB)_x(LiNbO_3)_{100-x}$ nanocomposite with the CoFe granules, elongated in the direction of nanocomposite growth up to 10–15 nm and with a lateral size of 2–4 nm [10, 11]. However, the $(CoFeB)_x(LiNbO_3)_{100-x}$ nanocomposite films have uniform thickness and follow the logarithmic law of thermal resistivity [10, 11]. The growth anisotropy of the Co–$LiNbO_3$ nanocomposite is apparently associated with the possibility of formation of an additional equilibrium phase of $LiCoO_2$ and, as a consequence, with the manifestation of unusual nucleation effects. High-resolution images with following Fast Fourier Transform analysis indicated that Co grains in the bottom part of the film do not correspond to cubic Co.

The presence of tightly packed granules in the lower part of the $(Co)_x(LiNbO_3)_{100-x}$ film and large particles in the upper part determines the ferromagnetic properties of the structure and its MR anisotropy. As can be seen from Fig. 9, intergranular gaps in the upper part of the film are considerably large (~5 nm), hence strong tunnel coupling between granules is excluded. Under these conditions, conductivity will be mainly determined by a hopping transfer along localized defects of amorphous matrix, which is commonly determined by the Mott's "$T^{1/4}$" law. For the lower part of the nanocomposite with the elongated granules, the so-called "oblique tunneling" with the subsequent transport of electrons along the chains of elongated granules appears to be crucial [7]. Conductivity of the relatively small part with elongated granules can be comparable or even higher than conductivity of the isotropic part of the nanocomposite. Therefore, the total conductivity is described neither by "$T^{1/2}$" nor "$\ln T$" laws. The high value of permittivity (ϵ_d ~ 50 [12]) of amorphous $LiNbO_3$ decreases the energy of the Coulomb blockade, and hence decreases possible value of LPMR during tunneling between granules in the lower part of the nanocomposite. Besides, shunting effect of the upper part is also important. Thus, the observed MR behavior of the given nanocomposite is mainly determined by the properties of its structure.

4. CONCLUSIONS

Along with the negative magnetoresistance (MR), associated with the spin-dependent tunneling, a linear positive MR (LPMR) is observed in the nanocomposites near the percolation threshold at low temperatures and in magnetic fields above the saturation field. In the nanocomposites $(Co)_x(SiO_2)_{100-x}$ (x = 65 at %) and $(CoNbTa)_x(SiO_2)_{100-x}$ (x = 58.5 at %) with a strong tunnel coupling between granules, characterized by a logarithmic temperature dependence of resistivity, the LPMR at T = 4.2 K is 0.03% and 0.06% T^{-1}, respectively. The developed simple theory of the LPMR for these nanocomposites, based on the influence of the Zeeman effect on the tunneling barrier height in the spin-dependent tunneling, makes it possible to qualitatively explain the results. The MR of $(Co)_x(LiNbO_3)_{100-x}$ (x = 49 at %) nanocomposite is anisotropic, and the LPMR at T = 50 K is about 10^{-3}% T^{-1} that is associated with the formation of the columnar structure at the initial stage of growth of this film.

FUNDING

This work was partially supported by the Russian Foundation for Basic Research (grant no. 19-07-00471) and by the Academy of Finland (grants nos. 333805 and 318405).

CONFLICT OF INTEREST

The authors declare that they have no conflicts of interest.

REFERENCES

1. A. Gerber, I. Kishon, I. Y. Korenblit, O. Riss, A. Segal, M. Karpovski, and B. Raquet, Phys. Rev. Lett. **99**, 027201 (2007).
2. M. Blinov, M. Shakhov, V. Rylkov, E. Lähderanta, V. Prudnikov, S. Nikolaev, A. Sitnikov, and A. Granovsky, J. Magn. Magn. Mater. **469**, 155 (2019).
3. V. Rylkov, S. Nikolaev, K. Y. Chernoglazov, V. Demin, A. Sitnikov, M. Y. Presnyakov, A. Vasiliev, N. Perov, A. Vedeneev, Y. E. Kalinin, et al., Phys. Rev. B **95**, 144202 (2017).

4. V. V. Rylkov, V. A. Demin, A. V. Emelyanov, A. V. Sitnikov, Y. E. Kalinin, V. V. Tugushev, and A. B. Granovsky, in *Novel Magnetic Nanostructures* (Elsevier, Amsterdam, 2018), p. 427.
5. E. Lähderanta, M. Guc, M. Shakhov, E. Arushanov, and K. Lisunov, J. Appl. Phys. **120**, 035704 (2016).
6. V. Rylkov, A. Emelyanov, S. Nikolaev, K. Nikiruy, A. Sitnikov, E. Fadeev, V. Demin, and A. Granovsky, J. Exp. Theor. Phys. **131**, 160 (2020).
7. I. Beloborodov, A. Lopatin, V. Vinokur, and K. Efetov, Rev. Mod. Phys. **79**, 469 (2007).
8. B. Abeles, P. Sheng, M. Coutts, and Y. Arie, Adv. Phys. **24**, 407 (1975).
9. J. Inoue and S. Maekawa, Phys. Rev. B **53**, R11927 (1996).
10. V. Rylkov, A. Sitnikov, S. Nikolaev, V. Demin, A. Taldenkov, M. Y. Presnyakov, A. Emelyanov, A.Vasiliev, Y. E. Kalinin, A. Bugaev, et al., J. Magn. Magn. Mater. **459**, 197 (2018).
11. V. Rylkov, S. Nikolaev, V. Demin, A. Emelyanov, A. Sitnikov, K. Nikiruy, V. Levanov, M. Y. Presnyakov, A. Taldenkov, A. Vasiliev, et al., J. Exp. Theor. Phys. **126**, 353 (2018).
12. T. Mitsuyu and K. Wasa, Jpn. J. Appl. Phys. **20**, L48 (1981).